ELSEVIER

Polymer 42 (2001) 1429–1439

polymer

www.elsevier.nl/locate/polymer

Study of the transition from Fickian to Case II sorption kinetics in the system poly(ethyl methacrylate)–liquid methyl alcohol

M. Sanopoulou*, D.F. Stamatialis[1]

Physical Chemistry Institute, Demokritos National Research Center, GR-15310 Aghia Paraskevi, Athens, Greece

Received 8 June 2000; accepted 23 June 2000

Abstract

Unidimensional transport of liquid methyl alcohol in poly(ethyl methacrylate) films at 30, 22, 10 and −5°C are presented. Kinetics of penetration, under semi-infinite conditions, are supplemented by information on the penetrant concentration profile obtained by an interferometric technique applied to the swelling polymer in situ. At 30°C, the system exhibits Fickian behavior. As the temperature is lowered, increasing deviations from Fickian kinetics are observed, with the end result of Case II kinetics at −5°C. The experimentally observed change in transport behavior is also predicted from diffusion Deborah numbers, calculated on the basis of the free volume theory of Vrentas and Duda. © 2000 Elsevier Science Ltd. All rights reserved.

Keywords: Case II kinetics; Poly(ethyl methacrylate); Diffusion Deborah number

1. Introduction

In a particular glassy polymer film–organic penetrant system, a variety of deviations from Fickian sorption kinetic behavior can usually be observed when the temperature and/or the external penetrant activity of the experiment is varied (e.g. Refs. [1–4]). In conventional vapor sorption (weight gain) experiments, the effect of these two variables can be studied separately. Furthermore, variation of the vapor pressure (activity) of the penetrant in the external phase at constant temperature according to different experimental protocols (e.g. by performing series of "integral" or "interval" sorption runs [2,4]) provides access to a wide variety of of non-Fickian sorption kinetics. In weight gain or penetration experiments with a liquid penetrant, one is limited to unit external activity and, due to the thermally activated nature of the sorption process, variation of the temperature of the experiment, also usually produces different penetrant concentration levels in the polymer. However, one has the advantage that, in experiments of this type, information on the penetrant concentration profile can be conveniently obtained by a variety of techniques [1,5–7], which may often be applied to the swelling film in situ [5–7].

In liquid penetration experiments, where a penetrant front advancing into the polymer can be observed, a simple descriptive way to quantify deviations from Fickian kinetics is possible on the basis of the power law:

$$X_p = kt^m \tag{1}$$

where X_p is the distance covered by the penetrant front at time t and k and m are constants. Under semi-infinite medium conditions, Fickian (Case I) kinetics is characterized by $m = 0.5$. Increasing values of m then denote increasing deviations from Fickian kinetics with $m = 1$ for Case II diffusion.

Non-Fickian sorption kinetics is most commonly attributed to slow viscous molecular relaxations of the glassy polymer structure (in response to penetrant-induced osmotic stresses), which occur on time scales comparable with that of the diffusion process [2,3,8–12]. However, detailed modeling work has shown that the build-up (and subsequent decay) of mechanical differential swelling stresses (arising from the non-uniform distribution of sorbed penetrant in the polymer sample during the sorption experiment) can also give rise to non-Fickian behavior [3,13,14]. This finding is supported by the experimental demonstration of deviations from Fickian sorption kinetics in the absence of relaxation processes [4,15,16]. In the presence of relaxation effects, the non-Fickian behavior can be discussed in terms of a dimensionless parameter, which may be defined either as the ratio of relaxation and effective diffusion rate constants (follow-

* Corresponding author. Tel.: +30-1-650-3785; fax: +30-1-651-1766.
E-mail address: sanopoul@mail.demokritos.gr (M. Sanopoulou).
[1] Present address: European Membrane Institute — Twente, University of Twente, Chemical Technology Department, P.O. Box 217, NL-7500 AE Enschede, The Netherlands.

PII: S0032-3861(00)00494-8

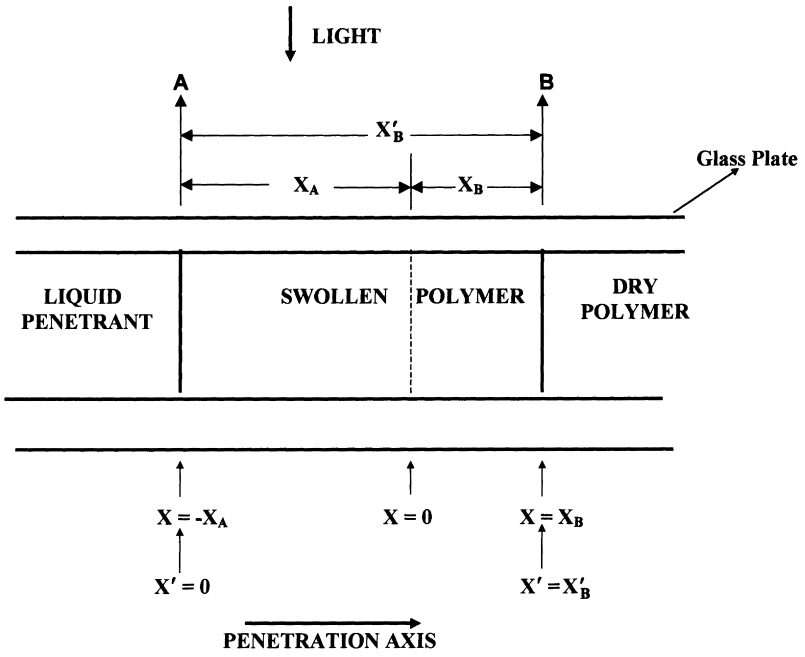

Fig. 1. Schematic presentation of experimental device illustrating distance coordinates X and X' (see text).

ing Crank [3]) or as the ratio of the characteristic relaxation and diffusion times (following Vrentas et al. [17]). The latter parameter, which is the reciprocal of the former, is referred to as the diffusion Deborah (DEB) number. Both parameters can be used to define the conditions under which non-Fickian behavior is expected to occur. Thus at high concentrations and/or temperatures, where the polymer–penetrant mixture is well above T_g, molecular relaxation is much faster than diffusional transport and Fickian diffusion in the fully relaxed polymer is observed characterized by DEB $\ll 1$. At sufficiently low temperatures and/or concentrations, where the system is well within the glassy state and behaves purely elastically, Fickian kinetics is again observed, characterized by DEB $\gg 1$. Deviations from Fickian kinetics are expected at intermediate values of DEB (a reasonable range would be between 0.01 and 100 [18]), where the system behaves viscoelastically (viscoelastic diffusion). Under appropriate conditions, which will be discussed in a subsequent section, Case II kinetics can be observed, characterized by a sharp penetrant front that advances into the polymer linearly with time, and by small concentration gradient in the swollen polymer behind the front. The most thoroughly studied experimental system is poly(methyl methacrylate)–liquid methyl alcohol [1], which exhibits Case II behavior at ambient and sub-ambient temperatures, but tends to deviate increasingly towards Fickian kinetics as the temperature is raised. However, a pure Fickian regime is not reached at the highest temperature limit imposed by the boiling point of the liquid penetrant.

Here we present a study of penetration of liquid methyl alcohol (MA) in poly(ethyl methacrylate) (PEMA) covering a large enough temperature interval to encompass the full range between Fickian and Case II kinetics. The concept of DEB number, calculated from material properties of the system, is applied to predict the observed changes in kinetic transport behavior.

2. Experimental

PEMA powder was obtained from Aldrich (code number 18208-7) with the following specifications: average $M_W =$ 515 K, $T_g = 63$°C, density 1.119 g/cm^3. MA was of analytical reagent grade.

Polymer films of thickness $l = 50$–100 μm were prepared by casting a 30% by wt acetone solution of the polymer powder on a glass surface. After formation, the film was removed from the glass plate and gradually heated in an oven to 70°C, maintained at that temperature for 24 h and finally returned gradually to room temperature. This heat treatment was followed by evacuation for at least one week.

Unidimensional penetration kinetics along one of the longitudinal directions of the film was studied by the following procedure [7]. A 3×5 mm^2 rectangular polymer sample was sandwiched between two glass plates, held together by spring clips. Before clamping, a thin ink mark was made on the film, in a region not to be reached by the penetrant during the experiment, to be used as reference point during the subsequent measurements. The sandwiched film was immersed in a bath of liquid MA, thermostated at the desired temperature. In this way, penetration across the film is prevented by the glass plates and can occur only along the film (Fig. 1). The glass plates had previously been smeared with a very thin film of silicon grease, in order to minimize friction and resistance to the back flow

Table 1
Transport parameters of the system PEMA–liquid MA, deduced from penetration and weight gain experiments at different experimental temperatures

Experimental temperature (°C)	Weight fraction of MA ($\omega_{1,F}$)	Volume fraction of MA ($\varphi_{1,F}$)	Interaction parameter (χ)	Exponent m of Eq. (1)	$dX_B/dt^{1/2}$ ($\times 10^2$) (mm/min$^{1/2}$)	$dX_A/dt^{1/2}$ ($\times 10^2$) (mm/min$^{1/2}$)	dX_B/dt ($\times 10^4$) (mm/min)	dX_A/dt ($\times 10^4$) (mm/min)
30	0.46 ± 0.01	0.54 ± 0.01	0.74 ± 0.01	0.53	7.0 ± 0.2	3.2 ± 0.1	–	–
22	0.38 ± 0.01	0.47 ± 0.01	0.80 ± 0.01	0.70	5.2 ± 0.1	2.0 ± 0.4	–	–
10	0.29 ± 0.01	0.37 ± 0.01	0.92 ± 0.01	0.82	3.5 ± 0.3	1.3 ± 0.1	–	–
−5	0.25 ± 0.01	0.32 ± 0.01	1.00 ± 0.01	0.99	–	–	5.2 ± 0.7	1.8 ± 0.5

of the swelling polymer along the penetration direction. Periodically, the sandwiched film, together with a sufficient amount of liquid MA, was quickly transferred from the bath to a Petri dish on the stage of a microscope (Amplival Pol-U of Jena). This technique allows in situ observation of the transport process under semi-infinite medium conditions, by means of suitable techniques. In particular, the edge of the film (swelling front A) and the penetrant front B (see Fig. 1), mark sharp changes in the concentration gradient and consequently in the mixture's refractive index gradient and are seen in the microscope as black lines. Their positions at time t were recorded, in terms of the distance coordinate X, using the position of the edge of the unswollen film at $t = 0$ as the origin (which was fixed relative to the ink mark). The relevant distances are represented by positive numbers X_A and X_B, respectively, while $X'_B = X_B + X_A$ represents the distance between fronts A and B, in terms of distance coordinate X' (Fig. 1).

The microscope was also equipped with a two-beam interferometric device, which permitted measurement of the variation of the optical path difference (OPD) profile along the direction of penetration [7,19]. The method involves measurement of lateral fringe displacements, $\Delta y(X')$, which corresponds to optical path differences between a location X' along the axis of penetration on the film specimen and a reference location, chosen within the pure liquid penetrant adjoining the edge of the film. The OPD profile, normalized in respect to the OPD of the dry polymer Δy_0, is given by

$$\frac{\Delta y(X')}{\Delta y_0} = \frac{n(X')\ell_X - n_1\ell_1}{n_2\ell_2 - n_1\ell_1} \tag{2}$$

In Eq. (2), n is the refractive index and ℓ the film thickness. The subscripts 1 and 2 refer to the pure liquid MA and dry polymer, respectively, and $n(X')$ and ℓ_x denote the refractive index and thickness of the swollen polymer at X'. Under conditions where the swelling polymer is constrained to a uniform thickness (i.e. $\ell_x = \ell_1 = \ell_2$), the OPD profile represents faithfully the refractive index profile $\Delta n(X')/\Delta n_0 = [n(X') - n_1]/[n_2 - n_1]$. If this condition is not valid, one may still determine the value of $n(X' = 0)$ at the swelling front (where $\ell_x = \ell_1$), by replacing the penetrant liquid with another immiscible liquid of known refractive index n'_1, measuring the new OPD value $\Delta y'(X' = 0)$ and solving the following equation:

$$\frac{\Delta y(X' = 0)}{\Delta y'(X' = 0)} = \frac{n(X' = 0) - n_1}{n(X' = 0) - n'_1} \tag{3}$$

In the absence of significant changes in volume upon mixing and for dilute solutions, a simple linear relation between the concentration C (expressed in mol per unit volume of solution) and n holds [19,20]:

$$\bar{V}_1 C(X') = 1 - \frac{\Delta n(X')}{\Delta n_0} \tag{4a}$$

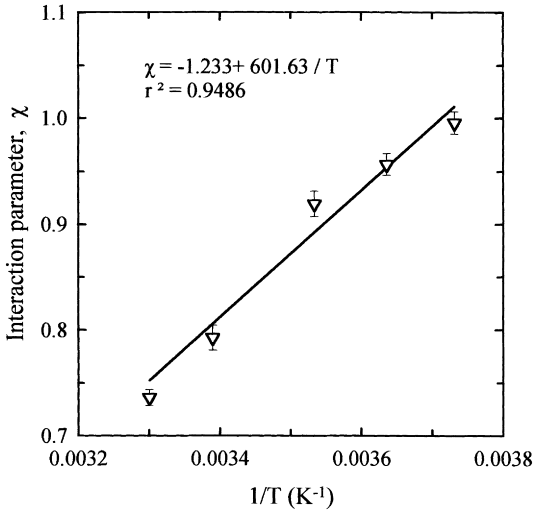

Fig. 2. Dependence of Flory–Huggins interaction parameter χ on temperature for the system PEMA–MA.

where $\bar{V}_1$ is the molar volume of pure penetrant. Hence, under conditions of uniform thickness, the concentration profile is related to the OPD profile as shown below:

$$\bar{V}_1 C(X') = 1 - \frac{\Delta y(X')}{\Delta y_0} \tag{4b}$$

Equilibrium weight gain measurements were performed by immersing dry preweighed polymer films in a thermostated bath of liquid MA. The samples were periodically removed from the bath, blotted with filter paper and weighed in stoppered bottles to constant weight. Samples equilibrated at −5°C were subsequently used to measure the T_g of the swollen polymer using a Dupont DSC 910 instrument at a heating rate of 10°C/min.

Tensile measurements on ca $60 \times 15 \times 0.07$ mm^3 dry polymer samples were performed at 22 ± 1°C using a tensile tester (Tensilon, type UTM-II-20, Toyo Baldwin Co). From stress–strain tests at a constant rate of elongation of 10 mm/min, a Young's modulus of 1.5 ± 0.1 GPa was determined and the strain limit of linear elastic behavior was found to be ~1%. Stress relaxation tests were performed well below this limit.

3. Results and discussion

3.1. Sorption equilibria

The equilibrium weight fractions $\omega_{1,F}$ of liquid MA in PEMA at various experimental temperatures, determined from weight gain measurements, and corresponding volume fractions $\varphi_{1,F}$ calculated assuming volume additivity upon mixing, are presented in Table 1.

According to the Flory–Huggins solution theory, $\varphi_{1,F}$ is related to the activity of the penetrant a by the following expression:

$$\ln a = \ln \varphi_{1,F} + (1 - \varphi_{1,F})(1 - 1/x) + \chi(1 - \varphi_{1,F})^2 \tag{5}$$

where the ratio of solvent to polymer molar volumes $1/x$, is negligible. Calculated values of the interaction parameter χ according to Eq. (5), using the aforementioned values of $\varphi_{1,F}$, are presented in Table 1 and plotted vs $1/T$ in Fig. 2. The temperature dependence of χ is expected to obey the relation

$$\chi = \chi_s + \bar{V}_1(\delta_1 - \delta_2)^2/RT$$

where χ_s is the entropic contribution to χ and δ_1, δ_2 are the solubility parameters of penetrant and polymer, respectively. Fig. 2 shows reasonable conformity to the expected linear dependence of χ on $1/T$. From the slope of this plot, in conjunction with values of $\delta_1 = 29.5$ J$^{1/2}$cm$^{-3/2}$ (the reported range for δ_1 is 29.2–29.7 J$^{1/2}$cm$^{-3/2}$ [21]) and $\bar{V}_1 = 40.5$ cm^3/mol, a value of $\delta_2 = 18.2$ J$^{1/2}$cm$^{-3/2}$ is derived. This value is within the range $18.2 - 18.7$ J$^{1/2}$cm$^{-3/2}$ of experimentally determined δ_2 values [21].

The positive values of χ at ambient temperatures are lower than the corresponding values of the poly(methyl methacrylate)–MA system [1,6], indicating that sorption of MA in PEMA is thermodynamically more favorable than in poly(methyl methacrylate).

3.2. Effect of temperature on penetration kinetics

The kinetic plots, describing the propagation of fronts A and B vs $t^{1/2}$ at 30, 22 and 10°C are presented in Fig. 3a–c. Data from at least three samples are included in each case to demonstrate the reproducibility of the results (which was usually substantially higher for the B front). At 30°C (Fig. 3a), the experimental data are best correlated by a straight line passing through the origin, in conformity with pure Fickian kinetics. As the experimental temperature is lowered, the penetration becomes slower and, more importantly, increasing deviations from Fickian kinetics are observed. At 22°C (Fig. 3b), this trend is evidenced by the fact that the best straight line through the data points does not pass through the origin. At 10°C (Fig. 3c), this deviation is much more pronounced. When the experimental temperature is further lowered to −5°C, a deterioration of the reproducibility of the measured penetration rate is observed, especially in the case of front A (Fig. 3d). The more reliable B data are best represented by kinetics which become linear when plotted on a t scale (Fig. 4), indicating clearly that Case II kinetics has been attained at −5°C. Representative X_B data from Fig. 3a–c, have also been replotted in Fig. 4 to show that Case II kinetics is not observed at higher temperatures.

As mentioned in Section 1, the deviations from Fickian kinetics in the intermediate cases can be quantified empirically through the exponent m of Eq. (1). The relevant ln–ln plots of Fig. 5 conform to Eq. (1) fairly well. The values of m deduced therefrom are presented in Table 1. As expected

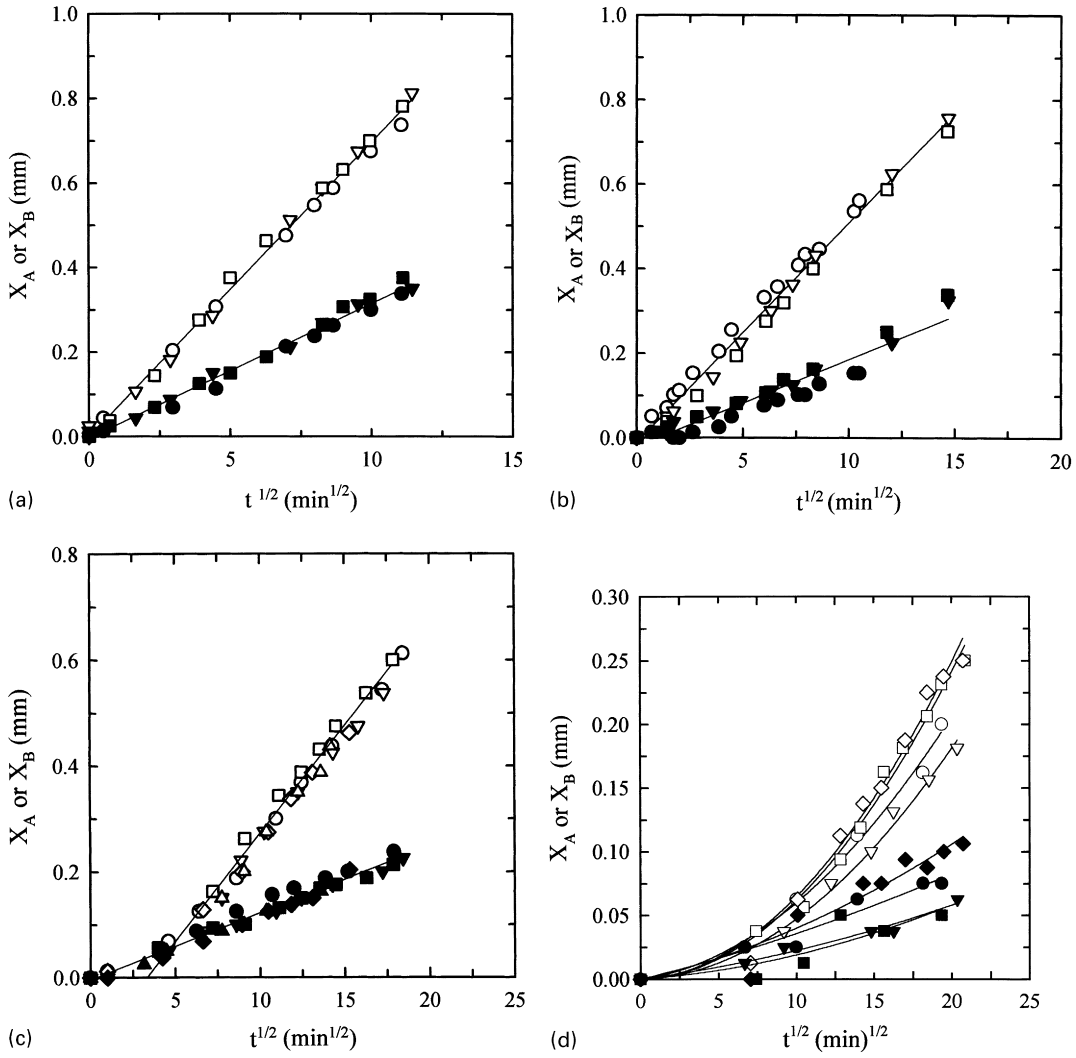

Fig. 3. Kinetics of swelling front A (filled points) and penetration front B (open points), plotted on $t^{1/2}$ scale, for longitudinal penetration of liquid MA into PEMA films at: (a) 30°C; (b) 22°C; (c) 10°C; and (d) −5°C.

$m \sim 0.5$ at 30°C, $m \sim 1$ at −5°C and at 22 and 10°C intermediate values of $m \sim 0.7$ and 0.8 are obtained.

Indicative penetration and swelling rates $dX_B/dt^{1/2}$ and $dX_A/dt^{1/2}$ were calculated from the linear part of Fig. 3a–c and mean values are presented at Table 1. Mean values of the penetration and swelling velocities dX_B/dt and dX_A/dt, deduced from the −5°C plots of Fig. 4 are also included in Table 1.

3.3. Effect of temperature on optical path difference profiles

Representative OPD profiles at all temperatures studied, for the same penetration distance X'_B, are shown in Fig. 6. They are, in each case, based on a considerable number of experiments in which the slope of the approximately linear part of the $\Delta y(X')/\Delta y_0$ vs X' profile in the swollen polymer region was measured directly. In all cases, there is a more or less abrupt rise of $\Delta y(X')/\Delta y_0$ near the dry polymer region, representing a corresponding drop in the penetrant concentration, which gives rise to the visible penetration front B. For the three higher temperatures, the decreasing sorptive capacity of the polymer with decreasing temperature is reflected in a correspondingly increasing $\Delta y(X' = 0)/\Delta y_0$ value at the swelling front A of the film. A similar rise in the $\Delta y(X' = 0)/\Delta y_0$ is not observed when the temperature is reduced from 10 to −5°C (Fig. 6). The relatively steep OPD profile in the swollen region at −5°C is also unexpected (although it is less steep than the corresponding profile at 10°C) because Case II transport is normally characterized by small concentration gradient behind the sharp penetration front. We believe that both the aforementioned anomalies are artifacts attributable to a non-uniform thickness of the film. As noted in Section 2, the OPD profile should reflect faithfully the refractive index profile only under the condition of uniform thickness. This condition is expected to be applicable in highly plasticized polymers. In this case, the deficit in overall swelling, due to the suppression of thickness swelling imposed by the confining glass plates and the

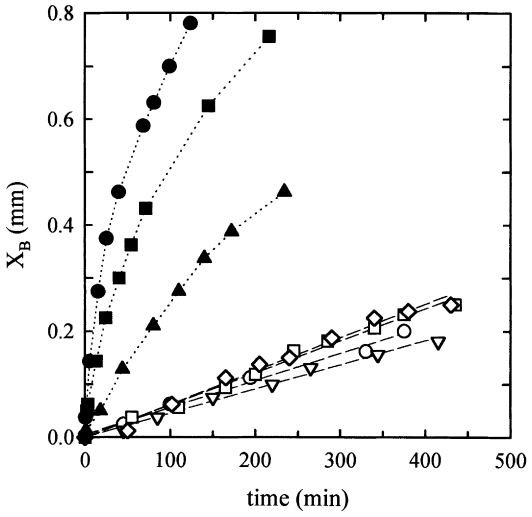

Fig. 4. Data of Fig 3d, on the propagation of front B at −5°C plotted here on a *t* scale (open points). Also included are corresponding representative B front data from Fig 3a (30°C, ●), Fig. 3b (22°C, ■) and Fig. 3c (10°C, ▲).

rigid unpenetrated region, can be made good by additional swelling along the axis of penetration (in the $-X$ direction) effected by plastic deformation [19]. On the other hand, a weakly plasticized polymer will be less prone to deform plastically in the $-X$ direction, and the resulting swelling pressure may be sufficient to push the glass plates apart to some extent, allowing a limited amount of dilation in the thickness direction [19]. The deformation of the swelling polymer in the $-X$ direction will be further hindered by friction against the confining glass plates. The suppression in swelling in the $-X$ direction is expected to become more severe as we move from front A towards front B, because (a) the decreasing concentration means that the polymer becomes more rigid and less deformable and (b) frictional

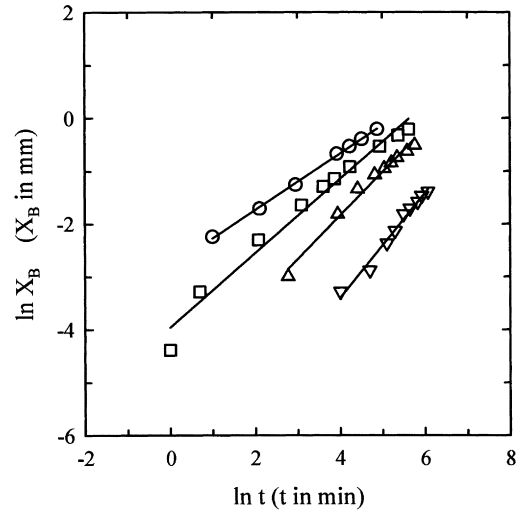

Fig. 5. Kinetic data of Fig. 4, replotted here on a double logarithmic scale. Values of the exponent, of Eq. (1), deduced from the respective slopes: $m =$ 0.53 (○, 30°C); 0.70 (□, 22°C); 0.82 (△, 10°C); 0.99 (▽, −5°C).

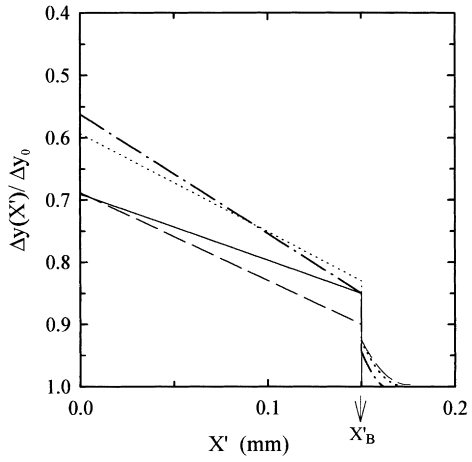

Fig. 6. Representative optical path difference, $\Delta y(X')/\Delta y_0$, profiles obtained during penetration of liquid MA in PEMA at: 30°C (·-·-·); 22°C (····); 10°C (- - -); −5°C(—).

resistance increases with X', since the polymer can swell at any X' only by pushing the swollen polymer between X' and A ahead of it. Effect (a) also impies a rise in swelling pressure and hence increasing tendency for some thickness dilation as we move from front A to front B. In this case, we expect $\Delta n(X' = 0)/\Delta n_0 > \Delta y(X' = 0)/\Delta y_0$ and a refractive index profile flatter than the OPD profile.

Measurement of the glass transition temperature of PEMA films equilibrated with liquid MA at −5°C, gave $T_g(C_F) \sim -10$°C. Hence full overall swelling at the swelling front A is reasonably expected. On the other hand, the fact that $T_g(C_F)$ is only slightly lower than the experimental temperature suggests that a strong effect (a) may also be reasonably anticipated, These expectations were confirmed by application of the two-liquid method of determining

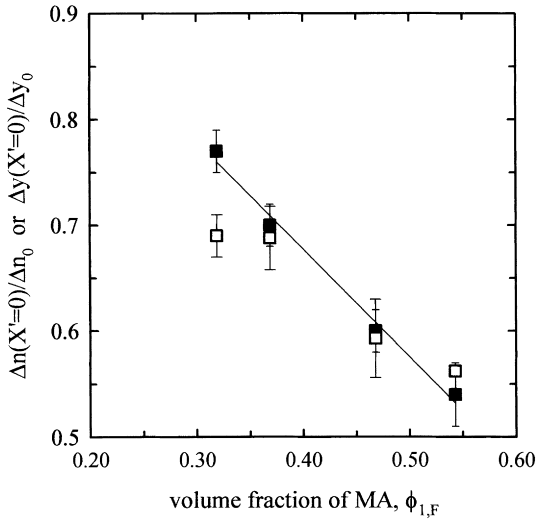

Fig. 7. Optical path differences $\Delta y(X' = 0)/\Delta y_0$ (□) and corresponding refractive index differences $\Delta n(X' = 0)/\Delta n_0$ ■, determined from OPD profiles at different experimental temperatures, vs the respective volume fractions $\varphi_{1,F}$ determined from equilibrium weight gain measurements.

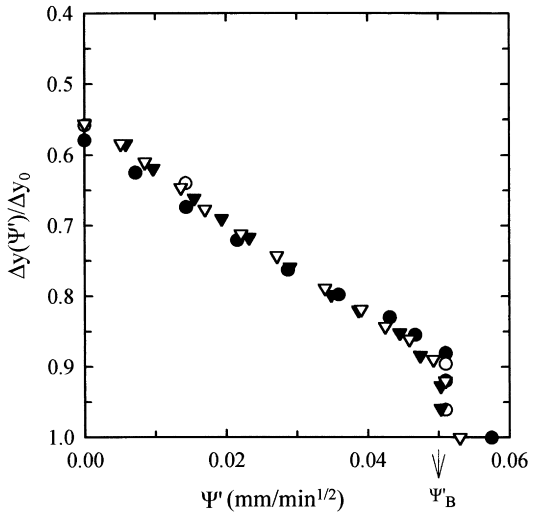

Fig. 8. Detailed optical path difference profiles obtained at different distances X'_B during penetration of MA in PEMA at 30°C, plotted on a $\Psi' = X'/2t^{1/2}$ scale. Penetration distance X'_B: 0.18 mm (●); 0.25 mm (○); 0.325 mm (▽); 0.375 mm (▼).

$n(X' = 0)$, described in the experimental method, using dibutyl phthalate as the second liquid. The corresponding $\Delta n(X' = 0)/\Delta n_0$ and $\Delta y(X' = 0)/\Delta y_0$ values for all temperatures studied are plotted vs the corresponding $\varphi_{1,F}$ values in Fig. 7, which reveals a very good linear correlation between $\Delta n(X' = 0)/\Delta n_0$ and $\varphi_{1,F}$. Furthermore, the $\Delta y(X' = 0)/\Delta y_0$ values for the three higher $\varphi_{1,F}$ values (and hence temperatures) fall practically on the same line, indicating that the assumption of uniform thickness is valid in these cases. At −5°C, the difference between the $\Delta n(X' = 0)/\Delta n_0$ and the $\Delta y(X' = 0)/\Delta y_0$ values corresponds roughly to a film thickness at the swelling front A ca 7% lower than that of the unpenetrated region near front B. This discrepancy may reasonably be expected to increase with penetration distance. In keeping with this, consecutive OPD measurements on the same sample at different increasing penetration distances X'_B gave increasing values of $\Delta y_0 = n_2\ell_2 - n_1\ell_1$. Thus, both the apparent anomalies, identified above, can be accounted for.

With respect to the Fickian regime, the conclusion of pure Fickian behavior at 30°C, drawn from the penetration kinetics of Fig. 3a, is confirmed by showing (Fig. 8) that the relevant OPD profiles $\Delta y(0 < X' < X'_B)/\Delta y_0$ (and hence the corresponding concentration profiles) measured at different penetration distances X'_B, coincide when plotted on a $\Psi' = X'/2t^{1/2}$ scale. It is experimentally very difficult to obtain information about these profiles in the region $\Psi' > \Psi'_B$. In any case, it is very doubtful if any such information would be useful, because of the probable breakdown of the linear relation between n and C at low C, which tends to sharpen the OPD profile [7], on one hand. On the other hand, the fact that some swelling pressure needs to develop, in order to overcome resistance to the propagation of swelling front A means that swelling at low C tends to be suppressed, thus slowing down diffusion and distorting the concentration profile in the $\Psi' > \Psi'_B$ region. Bearing in mind these limitations, diffusion coefficients can be derived from the OPD profiles of Fig. 8. These profiles can be converted to concentration profiles by the following relation derived from Eq. (4b):

$$C(\Psi') = C(\Psi' = 0)\frac{1 - \dfrac{\Delta y(\Psi')}{\Delta y_0}}{1 - \dfrac{\Delta y(\Psi' = 0)}{\Delta y_0}}$$

The concentration at the edge of the film $C(\Psi' = 0)$ is set equal to the value determined from equilibrium weight gain experiments at 30°C according to $C(\Psi' = 0) = C(X' = 0) = \varphi_{1,F}/\bar{V}_1$. According to Matano's formula [22a]

$$D[C(\Psi')] = -2\frac{\partial \Psi'}{\partial C}\int_0^{C(\Psi')} \Psi' \, dC \qquad (6)$$

For the particular shape of the OPD (and concentration) profiles of Fig. 8, and in the concentration range $C(\Psi' = 0) < C(\Psi') < C(\Psi' = \Psi'_B)$. Eq. (6) can be approximated by

$$D[C(\Psi')] = \frac{\Psi'_B}{C(\Psi' = 0) - C(\Psi'_B)}$$

$$\times\left\{[C(\Psi' = 0) - C(\Psi'_B)]\Psi'_B - [C(\Psi' = 0) - C(\Psi')]\Psi'\right\}$$

The D values derived by the above procedure (corresponding to the mutual diffusion coefficient as defined by Vrentas and Duda [23]) were found to vary from 6.7×10^{-7} cm^2/s at $C(\Psi' = 0)$ (corresponding weight fraction $\omega_{1,F} = 0.46$) to 3.1×10^{-7} cm^2/s at $C(\Psi' = \Psi'_B)$ (corresponding calculated weight fraction at front B, $\omega_{1,B} = 0.10$).

We also applied the treatment previously adopted in Ref. [7], wherein diffusion in the region $0 < \Psi' < \Psi'_B$ is described by a mean value of the diffusion coefficient $\bar{D}$ much higher than that prevailing in the $\Psi' > \Psi'_B$ region. In Ref. [7] only a limiting form of the solution for this case was given. The general solution is [22b]:

$$\Delta C = \frac{C(\Psi' = 0) - C(\Psi'_B)}{C(\Psi'_B)}$$

$$= \sqrt{\pi}\frac{\Psi'_B}{\sqrt{\bar{D}}}\exp\left(\frac{\Psi'^2_B}{\bar{D}}\right)\mathrm{erf}\left(\frac{\Psi'_B}{\sqrt{\bar{D}}}\right)$$

From the experimental value of ΔC, $\Psi'_B/\sqrt{\bar{D}}$,was read from Fig. 13.6 of Ref. [22b]. The experimental value of $\Psi'_B = X'_B/2\sqrt{t}$ (Fig. 8) then yielded a value of $\bar{D} = 5.3 \times 10^{-7}$ cm^2/s, within the range of diffusion coefficients determined above by Matano's method.

3.4. Calculation of DEB numbers

From the results presented so far, it is clear that in the

range 30 to −5°C, the system liquid MA–PEMA covers the whole range from Fickian to Case II kinetics. It is of interest to see if, for the penetration distances studied, DEB numbers calculated from material properties of the system can predict this variation in the transport behavior of the system.

DEB at given T, ω_1 is defined as [17]:

$$\mathrm{DEB}(T,\omega_1) = \tau(T,\omega_1)/\theta(T,\omega_1)$$

where τ is a characteristic relaxation time and θ a characteristic diffusion time of the mixture.

For the penetration experiments of the type described here, where the polymer substrate behaves throughout as a semi-infinite medium, θ is given by [14]:

$$\theta = \frac{(X'_{Bm})^2}{D}$$

where $X'_{Bm}$is the maximum distance attained by front B in each experiment and D is the mutual diffusion coefficient as defined by Vrentas and Duda [23].

For experiments covering small concentration intervals, the average value of DEB is sufficient to characterize the system. For experiments of the type described here covering significantly larger concentration intervals, where strong concentration dependence of both D and τ occurs, a mean DEB number is not sufficient to characterize the system's transport behavior. In these cases, we should take into account the values of DEB numbers characterizing (a) the initial (dry) and the final (swollen) state, designated as $\mathrm{DEB_I}$ and $\mathrm{DEB_F}$, respectively, and (b) the relative times of relaxation in the initial state and diffusion in the final state, designated as $\mathrm{DEB_R}$ (also termed integral DEB number [11]):

$$\mathrm{DEB_I}(T) = \tau(T,\omega_1=0)D(T,\omega_1=0)/(X'_{Bm})^2 = \tau_I(T)D_I(T)/(X'_{Bm})^2$$

$$\mathrm{DEB_F}(T) = \tau(T,\omega_1=\omega_{1,F})D_F(T,\omega_1=\omega_{1,F})/(X'_{Bm})^2 = \tau_F(T)D_F/(X'_{Bm})^2$$

$$\mathrm{DEB_R}(T) = \tau_I(T)D_F/(X'_{Bm})^2$$

For a sorption experiment characterized by both $\mathrm{DEB_I}$ and $\mathrm{DEB_F}$ much lower or much higher than unity, Fickian diffusion in the fully relaxed and unrelaxed polymer, respectively, is expected. Anomalous behavior is mainly characterized by intermediate values of $\mathrm{DEB_I}$. The particular conditions for the occurrence of a sharp penetration front advancing linearly with time (Case II transport), under semi-infinite conditions, are [14]:

(i) $\mathrm{DEB_I} \backsim 1$,
(ii) $\mathrm{DEB_F} \ll 1$ and
(iii) $\mathrm{DEB_R} \gg 1$

The first condition ensures that relaxation and diffusion at the front occur at comparable time scales, so that the former process is slow enough (but within experimental scales) in order to control the kinetics of penetration. The second condition implies that relaxation at the highly swollen region is sufficiently fast to ensure a practically fully relaxed polymer behind the sharp penetration front. The third, and most important [11], condition then ensures absence of diffusion limitations (and hence a flat concentration profile) so that the sharp front advances at a rate controlled by τ_I.

Calculation of D values was based on the free volume theory of Vrentas and Duda on the concentration and temperature dependence of the self diffusion coefficient.

D is related to the self-diffusion coefficient of the penetrant D^* by [24]:

$$D(T,\omega_1) = D^*(T,\omega_1)(1-2\chi\varphi_1)(1-\varphi_1)^2 \tag{7}$$

D^* is given by [23]:

$$D^*(T,\omega_1) = D_{01}\exp\left\{-\frac{\gamma(\omega_1\hat{V}_1^* + \omega_2\xi\hat{V}_2^*)}{\hat{V}_{FH}(T,\omega_1)}\right\} \tag{8}$$

In Eq. (8), which is also applicable for $\omega_1 = 0$, $\hat{V}_1^*$ and $\hat{V}_2^*$ are the specific critical local hole free volumes for penetrant and polymer respectively, required for a jump to a new position; $\hat{V}_{FH}(T,\omega_1)$ is the specific average hole free volume of the mixture; γ is the free volume overlap factor; ω_2 represents the weight fraction of polymer; and D_{01} is a constant, which is considered to be a property of the solvent only [24]. The parameter ξ is the ratio of the molar volume $\bar{V}_{1j}$ of a solvent jumping unit to the molar volume $\bar{V}_{2j}$ of a polymer jumping unit. For small solvent molecules that are expected to move as single units, ξ is defined as [24]

$$\xi = M_1\hat{V}_1^*/\bar{V}_{2j} \tag{9}$$

where M_1 is the molecular weight of pure MA. Both D_{01} and ξ are treated as constants, independent of temperature (as well as of concentration) both above and below T_g [25,26].

For $T > T_g$, $\hat{V}_{FH}/\gamma$ is given by [24,27]:

$$\frac{\hat{V}_{FH}(T>T_g,\omega_1)}{\gamma} = \omega_1\left(\frac{k_{11}}{\gamma}\right)(k_{21}+T-T_{g1}) + \omega_2\left(\frac{k_{12}}{\gamma}\right)\times(k_{22}+T-T_{g2}) \tag{10}$$

where T_{g1}, T_{g2} are the glass transition temperatures of penetrant and polymer, respectively, and k_{11}, k_{12}, k_{22} and k_{21} are related to the WLF equation constants of the two components. Since $T_g(C)$ of the equilibrated polymer–penetrant mixture was found to be ~ -10°C at the lower experimental temperature studied (−5°C), Eq. (10) was used for the calculations of D_F (as well as of τ_F below) at all experimental temperatures.

In contrast, for $\omega_1 = 0$, D_I and τ_I, correspond to the glassy state. In this case, $\hat{V}_{FH}/\gamma$ is given by [26,27]:

$$\frac{\hat{V}_{FH}(T<T_g,\omega_1=0)}{\gamma} = \frac{k_{12}}{\gamma}[k_{22}+\lambda(T-T_{g2})] \tag{11}$$

Table 2
Free volume theory parameters for the system PEMA–MA

PEMA	MA	PEMA–MA
$k_{22} - T_{g2} = -269.5$ K[a]	$k_{21} - T_{g1} = -47.9$ K[b]	$\xi = 0.253$[c]
$K_{12}/\gamma = 3.4 \times 10^{-4}$ cm^3/gK[a]	$K_{11}/\gamma = 1.17 \times 10^{-3}$ cm^3/gK[b]	
$\hat{V}_2^* = 0.915$ cm^3/g[a]	$\hat{V}_1^* = 0.963$ cm^3/g[b]	
$\lambda = 0.34$[d]	$D_{01} = 1.7 \times 10^{-3}$ cm^2/s[e]	

[a] From Ref. [24].
[b] From Ref. [28].
[c] Determined through Eqs. (9) and (12).
[d] From Ref. [26].
[e] From Ref. [25].

where λ is roughly the difference of the volume expansion coefficients of the polymer above and below T_g. The parameters in Eqs. (8)–(11) for the PEMA–MA system are listed in Table 2. All of them, except ξ, were found in literature [24–26,28]. Estimation of ξ was based on Eq. (9) in conjunction with the following empirical linear relationship [24]:

$$\bar{V}_{2j}(\text{cm}^3/\text{mol}) = 0.6224 T_{g2}(\text{K}) - 86.95 \quad (12)$$

A useful check on the applicability of the parameter values of Table 2 to our particular polymer–penetrant system, for temperatures above T_g, can be made by comparing the D_F and $D(\omega_{1,B})$ values derived from the OPD profiles of Fig. 8 at 30°C with the corresponding values calculated through Eqs. (7)–(10). The results, presented in Table 3, indicate that the experimental values approximate the theoretical ones to within a factor of ca 2. In addition, we checked the applicability of the parameters of Table 2 at temperatures below T_g, by comparing the experimental D_I values determined from the data of Ryskin (plot 2 of Ref. [29]) with the calculated ones through Eqs. (7), (8) and (11). The results, also given in Table 3 show that maximum discrepancy is observed at 30°C, where the experimental value is lower than the theoretical one by a factor of ~3.5. We consider the above comparisons quite satisfactory, given the approximations involved in the derivation of both the experimental and theoretical values. On the other hand, the parameters estimated with least accuracy are D_{01} and ξ [24]. Thus if we assume that the discrepancy between experimental and theoretical D values is due to an erroneous value of the D_{01}, a corresponding correction, based on experimental values of D, would result in an increase of all the calculated DEB numbers at most by a factor of 3.5. Such a correction would not alter the main conclusions drawn below.

In order to calculate DEB numbers, if a value of $\tau(T_{ref}, \omega_1 = 0)$ is known at a reference temperature T_{ref}, then $\tau(T, \omega_1)$ can be calculated by

$$\tau(\text{T}, \omega_1) = \tau(\text{T}_{ref}, \omega_1 = 0)\alpha_{TC}(\text{T}, \omega_1)$$

where α_{TC} is a shift factor.

Following Vrentas and Duda [30], α_{TC} is given by

$$\alpha_{TC}(T, \omega_1) \cong \frac{D_2^*(T_{ref}, \omega_1 = 0)}{D_2^*(T, \omega_1)} = \frac{\exp\left\{\dfrac{-\gamma \hat{V}_2^*}{\hat{V}_{FH}(T_{ref}, \omega_1 = 0)}\right\}}{\exp\left\{\dfrac{-\gamma(\omega_1 \hat{V}_1^* + \omega_2 \xi \hat{V}_2^*}{\hat{V}_{FH}(T, \omega_1)\xi}\right\}} \quad (13)$$

where D_2^* is the self-diffusion coefficient of the polymer.

Eqs. (7)–(13), in conjunction with the parameter values of Table 2, enable us to calculate DEB numbers for all the experimental temperatures studied, if a reference value of $\tau(T_{ref}, \omega_1 = 0)$ is known. The appropriate choice of $\tau(T_{ref}, \omega_1 = 0)$ is subject to discussion. As defined by Vrentas et al. [17], $\tau(T_{ref}, \omega_1 = 0)$ is the terminal relaxation time corresponding to the flow region of the viscoelastic spectrum. Durning et al. have used relaxation times corresponding to the transition time zone to predict non-Fickian behavior in the systems PMMA–methyl acetate vapor [8] and semicrystalline poly(ethylene terephthalate)–liquid solvents [31]. Here we first determined a terminal relaxation time from the stress-relaxation data of Nose and Hata [32] on PEMA at a reference temperature of 120°C. The corresponding DEB_I were found to be $\gg 1$ for all temperatures studied, indicating pure Fickian behavior, in contradiction to experimental evidence. We then performed stress relaxation experiments on our PEMA sample at 22°C. A reference temperature below T_g is most appropriate for present purposes because of the dependence of the viscoelastic spectrum of glassy polymers on the specific previous history of the sample [33]. From the representative stress relaxation curve, shown in Fig. 9, it is evident that at reasonable

Table 3
Comparison of experimentally determined D values with theoretical ones, calculated through Eqs. (7)–(11) in conjunction with parameter values of Table 2

Temperature (°C)	$D_F \times 10^6$ (cm^2/s)		$D(\omega_{1,B}) \times 10^6$ (cm^2/s)		$D_I \times 10^9$ (cm^2/s)	
	Experimental[a]	Theoretical	Experimenta;l[a]	Theoretical	Experimental[b]	Theor/cal
30	0.67	1.4	0.31	0.6	1.9	6.9
22					1.1	3.7
10					0.56	1.3

[a] This work.
[b] From Ref. [29].

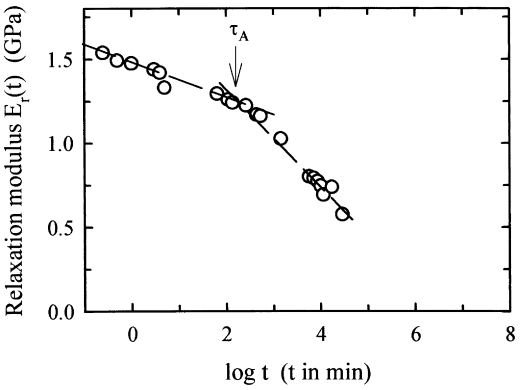

Fig. 9. Typical stress relaxation curve of dry PEMA at 22°C. The indicated time τ_A yields (assuming a box distribution of relaxation times) a value of the minimum relaxation time in the transition region $\tau = 1.78\ \tau_A$.

experimental time scales only the short time region of the transition zone is relevant. Accordingly, we deduced a mean value of $\tau(T_{ref} = 22°C,\ \omega_1 = 0) = 1.2 \times 10^4$ s corresponding to the short time part of the transition zone, assuming a box distribution of relaxation times [34]. The corresponding DEB numbers calculated for a max penetration distance $X'_{Bm} = 0.12$ cm, relevant to our experiments, are given in Table 4.

Our calculations revealed a much steeper dependence (i) of τ_I, as compared to D_I, on temperature and (ii) of τ, as compared to D, on concentration for a particular temperature (i.e. $\tau_F/\tau_I \ll D_I/D_F$). Table 4 shows that at 30°C both DEB_I and DEB_F are much lower than unity, indicating Fickian behavior in the fully relaxed polymer, in line with experimental observations. As the temperature is lowered, although DEB_F remain in all cases $\ll 1$, the DEB_I values become increasingly higher, mainly due to the increasingly higher τ_I values. At +10 and −5°C, DEB_I indicate anomalous viscoelastic behavior in line with the observed kinetics of Fig. 3c and d. On the other hand, the condition for Case II transport $DEB_R \gg 1$ is definitely satisfied only at −5°C.

Table 4
Calculated diffusion DEB numbers for the system PEMA–MA for different experimental temperatures and for a max penetration distance $X'_{Bm} = 0.12$ cm

Experimental temperature (°C)	DEB_I	DEB_F	DEB_R
30	3.7×10^{-4}	1.8×10^{-16}	8.1×10^{-2}
22	2.8×10^{-3}	1.3×10^{-15}	1.2
10	1.3×10^{-15}	3.6×10^{-14}	73
−5	11	3.6×10^{-14}	2.5×10^4

4. Conclusions

The main conclusions drawn from the present work are the following: (a) there is adequate experimental evidence that the system PEMA–MA in the temperature interval from 30 to −5°C, spans the range from purely Fickian to Case II transport and (b) the experimentally observed change is transport behavior can be predicted from diffusion DEB numbers calculated from material properties of the system.

In relation to (a), the kinetics of unidimensional penetration of MA in clamped PEMA films showed increasing deviations from Fickian behavior as the temperature was lowered from 30 to 22 and 10°C, with the end result of Case II kinetics at −5°C. The penetration kinetic data were supplemented by information on the penetrant concentration profiles obtained by an interferometric technique applied to the swelling polymer film in situ. The OPD profiles determined by this technique are expected to represent faithfully the corresponding refractive index (and hence concentration) profiles in the region of highly swollen polymer between the edge A of the film and the advancing penetrant front B, only under the condition of uniform film thickness. The present study, confirms our previous conclusions [19] that this condition is valid only when the swollen polymer is sufficiently plastisized in order to deform plastically along the axis of penetration and thus overcome the deficiency in overall swelling (due to the suppression of thickness swelling imposed by the confining glass plates and the rigid unpenetrated region). This case is best demonstrated here by the OPD profiles obtained at different penetration distances at 30°C which, in accordance with observed Fickian kinetics, were found to be coincident when plotted on a $X'/2t^{1/2}$ scale. Furthermore, diffusion coefficients deduced from these profiles by two different methods were in satisfactory agreement with calculated ones from free volume theory. Comparison of the OPD $[\Delta y(X' = 0)/\Delta y_0]$ and refractive index $[\Delta n(X' = 0)/\Delta n_0]$ values at the edge of film, indicates that the assumption of uniform thickness is also valid at 22 and 10°C, but not at −5°C, where $T_g(C_F)$ is only slightly lower than the experimental temperature. In this case, careful validitation of the OPD profile suggests that the corresponding concentration profile is more flat, as expected for Case II transport.

In relation to (b), because of the strong concentration dependence of the diffusion and relaxation processes, a mean value of DEB number is not adequate for the characterizion of the system's transport behavior. Accordingly we calculated DEB numbers corresponding to (i) the initial as well as the final state of the polymer, and (ii) the relative times of relaxation in the initial state and diffusion in the final state. The corresponding mutual diffusion coefficients and relaxation times were determined on the basis of the free volume theory of Vrentas and Duda using the parameter values found in literature in conjunction with a relaxation time deduced from stress relaxation experiments on dry polymer samples at a reference temperature of 22°C. On the basis of these calculations, a passage from Fickian to Case II kinetics is anticipated as the temperature is lowered from 30 to −5°C, in agreement with experimental evidence.

References

[1] Thomas N, Windle AH. Polymer 1978;19:255.
[2] Fujita H. Adv Polym Sci 1961;3:1.
[3] Crank J. J Polym Sci 1953;11:151.
[4] Sanopoulou M, Roussis PP, Petropoulos JH. J Polym Sci, Part B: Polym Phys 1995;33:993.
[5] Mills PJ, Palmstrom CJ, Kramer EJ. J Mater Sci 1986;21:1479.
[6] Durning CJ, Hassan MM, Tong HM, Lee KW. Macromolecules 1995;28:4234.
[7] Sanopoulou M, Petropoulos JH. J Polym Sci, Part B: Polym Phys 1992;30:971.
[8] Durning CJ. J Polym Sci, Polym Phys Ed 1985;23:1831.
[9] Thomas N, Windle AH. Polymer 1982;23:529.
[10] Joshi S, Astarita G. Polymer 1979;20:455.
[11] Wu JC, Peppas NA. J Polym Sci Part B Polym Phys 1993;31:1503.
[12] Petropoulos JH. J Polym Sci, Polym Phys Ed 1984;22:1885.
[13] Petropoulos JH. J.Membrane Sci 1984;18:37.
[14] Petropoulos JH. J Polym Sci Polym Phys Ed 1984;22:183.
[15] Sanopoulou M, Petropoulos JH. Polymer 1997;38:5761.
[16] Samus MA, Rossi G. Macromolecules 1996;29:2275.
[17] Vrentas JS, Jarzebski CM, Duda JL. AIChE J 1975;21:894.
[18] Vrentas JS, Vrentas CM, Huang WJ. J Appl Polym Sci 1997;64:2007.
[19] Stamatialis DF, Sanopoulou M, Petropoulos JH. J Appl Polym Sci 1997;65:317.
[20] Heller W. J Polym Sci: Part A-2 1966;4:209.
[21] Van Krevelen DW. Properties of polymers. 3rd ed.. Amsterdam: Elsevier, 1990 (part VII).
[22] Crank J. Mathematics of diffusion. 2nd ed. London: Oxford University Press, 1975 (chaps 10 and 13).
[23] Vrentas JS, Duda JL. J Polym Sci 1977;15:403.
[24] Zielinski JM, Duda JL. AIChE J 1992;38:405.
[25] Vrentas JS, Vrentas CM. Macromolecules 1993;26:1277.
[26] Vrentas JS, Duda JL. J Appl Polym Sci 1978;22:2325.
[27] Vrentas JS, Vrentas CM. J Polym Sci, Part B: Polym Phys 1992;30:1005.
[28] Hassan MM, Durning CJ. J Polym Sci, Part B: Polym Phys 1999;37:3159.
[29] Ryskin GYA. J Tech Phys (USSR) 1955;25:458.
[30] Vrentas JS, Duda JL. J Polym Sci, Polym Phys Ed 1977;15:441.
[31] Billovits GF, Durning CG. Polymer 1988;29:1468.
[32] Nose T, Hata T. J Polym Sci: Part C 1967;16:2019.
[33] Ferry JD. Viscoelastic properties of polymers. 3rd ed. New York: Wiley, 1960 (chap 15).
[34] Tobolsky AV. Properties and structure of polymers. New York: Wiley, 1980 (chap 3).